Quantum-Assisted Measurement of Atomic Diamagnetism

Yaakov Y. Fein, Armin Shayeghi, Lukas Mairhofer, Filip Kiałka, Philipp Rieser, Philipp Geyer, Stefan Gerlich, and Markus Arndt*

Faculty of Physics, University of Vienna, Boltzmanngasse 5, A-1090 Vienna, Austria

(Received 23 August 2019; revised manuscript received 6 November 2019; published 22 January 2020)

We report the first measurement of ground-state diamagnetism of isolated neutral atoms in an atomic beam. We realize this measurement using magnetic deflection of fringes in a long-baseline matter-wave interferometer. The observed diamagnetic susceptibilities of $-5.8 \pm 0.2 \pm 0.4 \times 10^{-9}$ m^3/kg for barium and $-7.0 \pm 0.3 \pm 0.7 \times 10^{-9}$ m^3/kg for strontium are in good agreement with the theoretical values and correspond to a measured force on the order of 10^{-26} N. The high force sensitivity also allows us to observe the isotope dependence of the interference visibility due to the nuclear permanent magnetic moment, thereby demonstrating a new method for neutral isotope selection. The universality of the technique allows the magnetism of a wide range of atoms and molecules to be studied in the gas phase.

DOI: 10.1103/PhysRevX.10.011014

Subject Areas: Atomic and Molecular Physics, Magnetism

I. INTRODUCTION

Diamagnetism is a fundamental effect in all atoms and molecules, but it is often dwarfed by larger paramagnetic contributions to the susceptibility [1]. In bulk materials, the net susceptibility of both paramagnetic and diamagnetic materials can be measured using a variety of established methods, such as the Gouy or Evans balance, NMR shifts, and SQUID-based measurements.

Paramagnetism has also been observed on the single-particle level, as has been exploited in the famous Stern-Gerlach experiment [2], the Rabi resonance method [3], and routinely in atom cooling and trapping experiments [4]. Modern beam deflection methods are also sensitive to the paramagnetism of small clusters and molecules [5–10].

Single-particle diamagnetism, however, is typically much harder to measure due to the smallness of the effect. For high-vapor-pressure materials such as the noble gases and a few simple hydrocarbons, the diamagnetic susceptibility has been measured using gas balance techniques [11–13]. Diamagnetic susceptibilities of highly excited Rydberg states have also been reported for a range of metal atoms including barium [14,15], which is possible due to the scaling of the effect with the electron orbit radius.

Measurements on isolated particles are important because bulk magnetic properties can differ significantly from those of the constituent atoms or molecules. For example, the closed-shell alkaline-earth elements barium and strontium are paramagnetic in bulk due to Pauli paramagnetism but are predicted to be diamagnetic when isolated. While the bulk paramagnetic susceptibilities have been measured [16], the ground-state atomic susceptibilities of barium and strontium have not been experimentally accessible until now. The measurement of neutral strontium may be of particular interest to the atomic-clock community, which typically relies on a calculated diamagnetic correction to the nuclear g-factor [17].

Here, we report on a new technique to measure single-particle magnetic susceptibilities via fringe deflection in a matter-wave interferometer [18]. We use the Long-baseline Universal Matter-wave Interferometer (LUMI) [19], a three-grating near-field interferometer that can accept a wide range of atoms and molecules.

Various realizations of matter-wave interferometers have been employed with a range of atomic and molecular species in tests of fundamental physics and precision sensing [20]. Interferometers have also been used to measure electronic and optical properties of atoms and molecules [21–25], and here we extend this concept to atomic diamagnetism. The magnetic susceptibility manifests as a shift of the interference fringes due to the repulsive force on a small magnetic moment induced in a tailored magnetic field. The fringes can be monitored with nanometer resolution, which is what lends the technique its high sensitivity.

A permanent paramagnetic moment, on the other hand, is deflected in different directions, dependent on the projection of the magnetic moment onto the magnetic field axis. Averaging over an ensemble of atoms thus reduces the

*markus.arndt@univie.ac.at

interference visibility. We show the sensitivity of the experiment to a nonzero nuclear spin by comparing the interference visibilities of different isotopes.

Alkaline-earth and alkaline-earth-like elements have attracted significant interest in recent years for their potential use in precision measurements. Several strontium interferometers have been demonstrated [26–29], along with a range of other elements [30–33], with envisioned applications including gravimetry, gravitational wave sensing, and equivalence principle tests. The insensitivity to magnetic fields is one of the key benefits of working with such atoms. In the gravity gradiometer demonstrated in Ref. [29], the extremely low sensitivity of strontium to magnetic field gradients was demonstrated, although the sensitivity of this particular experiment was about 3 times too low to observe the diamagnetic contribution. In the current work, we measure this small diamagnetic term for strontium as well as for barium, which shares many of the appealing aspects for precision measurements.

II. EXPERIMENTAL SETUP

We demonstrate the technique with barium and strontium since they both form thermal atomic beams, have vanishing electron magnetic moments, and have several stable isotopes. A thermal atomic beam is formed in a ceramic oven held at 1000–1300 K. The atoms then traverse the three-grating interferometer (see Fig. 1) and a specially designed deflection magnet that can be moved in and out of the atomic beam with a vertical translation stage.

The LUMI deflectometry experiments rely on the Talbot-Lau effect in the scheme illustrated in Fig. 1. The Talbot-Lau effect [34,35] is a near-field self-imaging phenomenon first demonstrated with atoms [36] and later

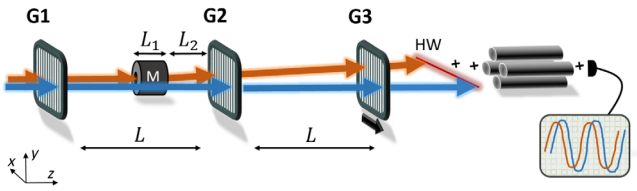

FIG. 1. The experimental setup showing the two modes of operation in our experiment. Blue arrows indicate the reference measurements, where atoms traverse the interferometer with the deflection magnet withdrawn from the beam; red arrows show the deflected paths of the atoms when the experiment is repeated with the beam passing through the magnet. The thermal barium beam enters from the left, passes the three gratings ($G1$, $G2$, $G3$) and the cylindrical deflection magnet (M), and is ionized by the hot rhenium wire (HW). The sinusoidal interference patterns are sampled by scanning $G3$ transversely. Here, L is the inter-grating separation (0.98 m), L_1 the length of the magnet (0.04 m), and L_2 the distance of the magnet edge from $G2$ (0.12 m).

with increasingly massive molecules [19,37]. The first grating $G1$ creates transverse coherence such that the second grating $G2$ is coherently self-imaged. This process produces a density pattern in the beam behind $G2$, which we sample by scanning a third grating $G3$ across the beam. We use the symmetric configuration in which each grating period is equal and the gratings are separated equidistantly. The modulation then has the grating period d and is strongest when the intergrating spacing L is approximately an integer multiple of the Talbot length, $L_T = d^2/\lambda_{\mathrm{dB}}$, with λ_{dB} the de Broglie wavelength. Typical values of L_T in the experiments presented here are of order one centimeter; hence, L is close to $100L_T$. The low collimation requirements of such a scheme permit higher throughput than a far-field interferometer with a similar baseline.

We use nanomechanical gratings with a period of 266 nm, which are compatible with the high beam velocities and relatively small polarizabilities of barium and strontium [38], where particle-grating interactions are weak. For slower and highly polarizable particles such as large molecules, $G2$ can be exchanged for an optical phase grating in the same experiment [19].

After traversing the interferometer, the atoms are ionized (see the Appendix for details), mass-selected by a quadrupole mass spectrometer (QMS), and counted with an electron multiplier.

III. DIAMAGNETIC DEFLECTION

For magnetic deflection experiments, we employ a retractable permanent deflection magnet positioned before the second grating. The magnet is a modified Halbach cylinder arrangement of 24 neodymium-iron-boron segments, each with a typical remanent magnetization of 1.29 T. It was designed to have a uniform $(\mathbf{B}\cdot\nabla)B_x$ field in a region near the cylinder axis [18]. Rectangular apertures at the entrance and exit of the magnet ensure that the atoms fly through a 2.00×0.75 mm^2 region of the magnet chosen to be large enough to permit significant flux while still sampling a force field sufficiently homogeneous to avoid strong dephasing. The magnet was characterized with a Hall probe, showing a peak $(\mathbf{B}\cdot\nabla)B_x$ field of 59 ± 5 T^2/m, falling off near the magnet edges, as shown in Fig. 2. The force within the magnetic cylinder over the selected region is constant to 9%.

The magnetic field induces a dipole moment $\boldsymbol{\mu} = (\chi_m m)\mathbf{B}/\mu_0$, with χ_m the mass magnetic susceptibility and m the particle mass, which leads to a force

$$F_x = (\boldsymbol{\mu}\cdot\nabla)B_x = \frac{m(\mathbf{B}\cdot\nabla)B_x}{\mu_0}\chi_m. \tag{1}$$

This force causes a transverse position and velocity shift of the atoms after traversing the magnet,

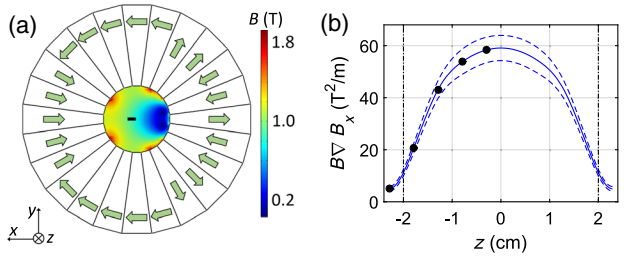

FIG. 2. (a) Pole arrangement of the 24 permanent magnet segments and simulated magnetic flux density map inside the hollow cylinder (16 mm inner diameter). The small black rectangle indicates the region traversed by the atoms. (b) The $(\mathbf{B}\cdot\nabla)B_x$ field over the traversed region as a function of longitudinal position as determined from Hall-probe measurements (black dots). The vertical black dashed lines indicate the extent of the magnet cylinder. The mirror symmetry of the magnet with respect to the $z=0$ plane has been used to extrapolate the fields for the spline fit shown in blue, where the blue dashed lines correspond to 1 standard deviation of the measured values, indicating the uniformity of the force field.

$$\Delta x_{\mathrm{mag}} = \int_0^{L_1}\int_0^{z'} \frac{F_x(z')}{m{v_z}^2}\,dz'dz, \qquad \Delta v_x = \int_0^{L_1}\frac{F_x(z)}{mv_z}\,dz. \tag{2}$$

The integrals of $F_x(z)$ are obtained numerically using the z dependence shown in Fig. 2. In the reference frame of the atoms, the second and third gratings are shifted by $\Delta x_2 = -\Delta x_{\mathrm{mag}} - \Delta v_x L_2/v_z$ and $\Delta x_3 = -\Delta x_2 - \Delta v_x L/v_z$, respectively. The phase shift of the interference pattern is then obtained by the formula [20,39] $\Delta\phi = k[\Delta x_1 - 2\Delta x_2 + \Delta x_3]$, where $\Delta x_1 = 0$ and $k = 2\pi/d$.

To account for the finite spread of velocities in the beam, one must average the interference pattern over the velocity distribution $\rho(v_z)$. The observed pattern $\overline{\mathrm{A}}\cos(kx+\overline{\Delta\phi})$ is an incoherent sum of the contributions of different velocity classes,

$$\overline{\mathrm{A}}\cos(kx+\overline{\Delta\phi}) = \int_0^\infty dv\rho A\cos(kx+\Delta\phi), \tag{3}$$

where A is the velocity-dependent fringe visibility. The velocity dependence of the amplitudes A is determined following the treatment in Ref. [40] for a retarded C4 potential. Its effect on the mean deflection is less than 5% for our parameters.

The velocity of the atomic beam was measured via cross-correlation with a pseudorandom chopper sequence and fitted to a skew normal distribution. Care was taken to account for the residence time of the atoms on the rhenium surface of the Langmuir-Taylor detector, as described in the Appendix, along with further details of the measured distributions.

Interference measurements were made with and without the $(\mathbf{B}\cdot\nabla)\mathrm{B}_x$ field to determine the relative phase shift induced by the deflection magnet. This process was done by mechanically moving the magnet in and out of the atomic beam with a vertical translation stage. The experiment was repeated several times to ensure that the observed phase shift was reproducible, as shown in Fig. 3. For barium, three consecutive interference scans were recorded with and then without the magnet; this sequence was repeated 4 times, for a total of 24 measurements. For strontium, six consecutive measurements were taken with and then without the magnet, for a total of 12 measurements.

The barium deflection data were taken with the QMS in a low-resolution mode to maximize the count rate, in which the various barium isotopes were not distinguished. For strontium, the high-resolution mode was used throughout, and for these deflection measurements, we selected the most abundant isotope, ^{88}Sr. The mean observed visibility of the barium (strontium) interference fringes without the magnet was 11.6% (13.8%), slightly below the expected visibility after taking into account Casimir-Polder dephasing at the second grating [40]. The barium (strontium) visibility was reduced to 7.2% (8.5%) upon insertion of the magnet.

The mean deflection of the barium fringes in Fig. 3 is 20.9 ± 0.7 nm. Solving Eq. (3) for this deflection and

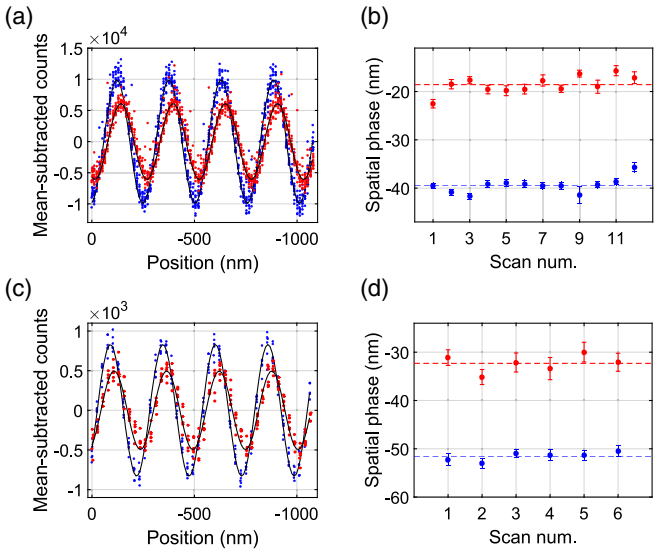

FIG. 3. (a) Barium interference patterns with (red) and without (blue) the deflection magnet, where solid curves are sine fits. Mean counts are subtracted to adjust for a small drop of the count rate during the measurement, and several outliers due to signal instabilities lie beyond the plotting region. A phase shift and contrast loss due to the magnet are both clearly visible. (b) The phase of each measurement, with dashed lines showing the mean values (red with magnet, blue without). Error bars are 1-σ confidence intervals of the phase. (c) Same as in panel (a), but for strontium. (d) Same as in panel (b), but for strontium.

finding the best-fit susceptibility yields $\chi_m(\mathrm{Ba}) = -5.8 \pm 0.2 \pm 0.4 \times 10^{-9}$ m^3/kg. Since the induced magnetic moment $\boldsymbol{\mu} = (\chi_m m)\mathbf{H}$, the susceptibility per atom, $\chi_m m$, is $-1.33 \pm 0.05 \pm 0.09 \times 10^{-33}$ m^3. The first error is the statistical error due to the standard error of the observed deflection, while the second error is systematic and is dominated by the uncertainty in the velocity distribution and $(\mathbf{B} \cdot \nabla)B_x$ field.

In a similar manner, the observed strontium deflection of 19.3 ± 0.7 nm yields a diamagnetic susceptibility $\chi_m(\mathrm{Sr}) = -7.0 \pm 0.3 \pm 0.7 \times 10^{-9}$ m^3/kg. The susceptibility per strontium atom is $-1.02 \pm 0.04 \pm 0.10 \times 10^{-33}$ m^3. To put this into context, the magnitude of the induced magnetic moment of a strontium atom in a 1-Tesla field is 4 orders of magnitude smaller than a single Bohr magneton.

We can compare the measured susceptibilities with values calculated using density functional theory with magnetic-field-dependent gauge-independent atomic orbitals (GIAOs) [41], as implemented in Gaussian16 [42]. We used the PBE0 exchange-correlation functional [43] and the def2-QZVPP basis set [44]. The method was benchmarked with xenon, which reproduced the measured value [13] to 2%. The isotropic susceptibilities were calculated as -6.17×10^{-9} m^3/kg for barium and -7.34×10^{-9} m^3/kg for strontium, in good agreement with the measured values. The ratio of the theoretical values, $\chi_m(\mathrm{Sr})/\chi_m(\mathrm{Ba}) = 1.19$, is in excellent agreement with the measured ratio of 1.19 ± 0.06, in which most of the systematic error cancels. The experimental values are both 6% smaller than the theoretical values, suggestive of a small systematic error.

IV. ISOTOPE-SELECTIVE INTERFERENCE

Operating the QMS in a high-resolution mode allows us to perform interference measurements on each of the three most abundant isotopes of barium and strontium, with and without the deflection magnet. Figure 4 shows the complete loss of interference visibility for the odd-numbered isotopes in the presence of the $(\mathbf{B} \cdot \nabla)B_x$ field. Without the magnet, full interference visibility is recovered for each of the isotopes.

Unlike the even-numbered isotopes, ^{137}Ba and ^{87}Sr carry a permanent magnetic moment due to an unpaired nuclear spin, with $I = 3/2$ for ^{137}Ba and $I = 9/2$ for ^{87}Sr. The permanent magnetic moment of ground-state ^{137}Ba is given by $\mu_z = g\mu_N m_I/\hbar = 0.94\mu_N$ for the $m_I = 1/2$ component [45], with four possible spin projections. The effect of a ∇B_x field on ^{137}Ba is, in general, a reduction of the interference visibility. Assuming a transversely constant ∇B_x (peak value of 77 T/m) and treating the four Stern-Gerlach branches as a classical mixture of trajectories (since the different spin states cannot interfere), the reduced barium fringe amplitude is

$$\overline{A} = \frac{1}{2}\left| \int_0^\infty dv_z \rho A[\cos(\Delta\phi_p) + \cos(3\Delta\phi_p)]e^{i\Delta\phi} \right|. \quad (4)$$

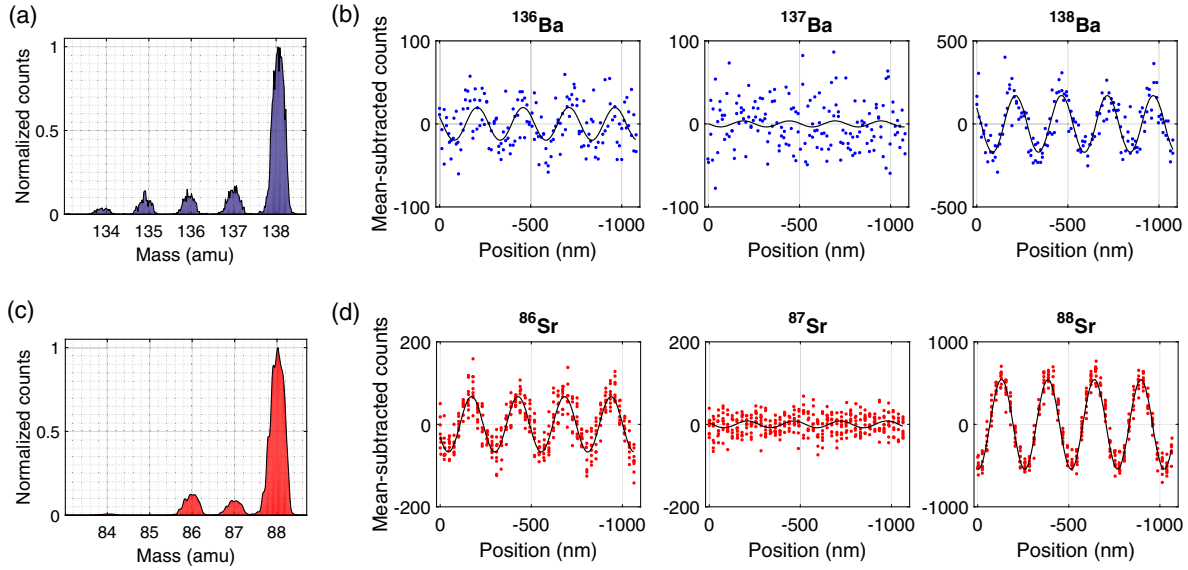

FIG. 4. (a) Measured isotope distribution of barium. Interference scans were performed with the QMS tuned to a particular isotope peak. (b) Interference of ^{136}Ba, ^{137}Ba, and ^{138}Ba, with the deflection magnet inserted. Solid curves indicate sine fits. Here, ^{137}Ba, with its unpaired nuclear spin, exhibits no contrast, while the even isotopes retain full contrast. (c) Measured isotope distribution of strontium. (d) Interference of ^{86}Sr, ^{87}Sr, and ^{88}Sr, with the deflection magnet inserted, showing even more clearly the loss of visibility for the odd-numbered isotope.

Here, $\Delta\phi_p$ is the paramagnetic shift of the $m_I = 1/2$ level, as obtained from Eq. (2) and the first part of Eq. (1) for a permanent magnetic moment $\boldsymbol{\mu}$. For generality, the diamagnetic shift $\Delta\phi$ has been included as well.

Equation (4) predicts a visibility loss greater than 85% for ^{137}Ba. This loss is a conservative estimate since in our magnet $(\mathbf{B}\cdot\nabla)\mathrm{B}_x$ is nearly constant and ∇B_x is not, resulting in additional spatial averaging. The observed loss of interference visibility is thus consistent with the presence of a permanent nuclear magnetic moment. Such an experiment can be operated without a QMS as a technique for neutral isotope selection, with the level of selectivity determined by the interference contrast.

V. CONCLUSION

The diamagnetic susceptibility of isolated barium and strontium atoms was measured via the shift of interference fringes in a long-baseline matter-wave interferometer. By mass-selecting the various isotopes, the presence of nuclear spin was observed through a loss of interference visibility for the odd-numbered isotopes with unpaired nuclear spins.

The universal nature of LUMI allows us to show interference with molecules as well as atoms. The addition of a constant gradient magnetic field in the setup will allow further studies of permanent magnetic moments, photoisomerization effects, and triplet-state lifetimes in complex molecules. The technique can also be used to purify nuclear isotopes for applications in spectroscopy.

ACKNOWLEDGMENTS

This project has received funding from the European Research Council (ERC) under the European Union's Horizon 2020 Research and Innovation Program (Grant No. 320694), and the Austrian Science Fund (FWF) within programs P-30176 and W1210-N25. The computational results presented were obtained using the Vienna Scientific Cluster (VSC) within Grant No. 70918. A. S. acknowledges funding by the FWF within the Lise-Meitner Grant No. M 2364.

APPENDIX: EXPERIMENTAL DETAILS

Langmuir-Taylor surface ionization from a heated rhenium wire was used to ionize the atoms after the interferometer. Alkaline-earth elements such as barium and strontium can exhibit residence times up to several seconds before desorption from a hot metal surface. To prevent a systematic error in time-of-flight measurements and a corresponding error in susceptibilities, we collected the spectra at a wire current of 5.8 A for barium and 6.0 A for strontium, corresponding to wire temperatures of 2550 K and 2590 K, respectively [46]. At these temperatures, the residence times for barium and strontium are estimated as 120 μs and 2 μs, respectively [47,48], short enough to have a minimal impact on velocity measurements, as confirmed by the convergence shown in Fig. 5. A small correction for barium was applied by deconvoluting the velocity spectrum with an exponential delay corresponding to the 120 μs residence time.

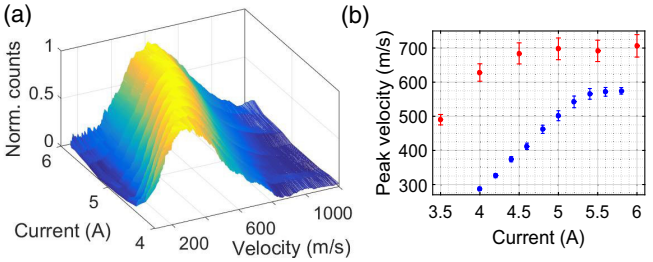

FIG. 5. (a) Velocity spectra as a function of hot-wire current for barium. (b) The convergence of the velocity spectra at high wire temperatures, seen by plotting the peak velocities of skew normal fits to the velocity data against the wire current. The blue marks show barium data; red marks are for strontium. Error bars are from 1-σ confidence intervals of the velocity calibration.

Skew normal distributions were used for fitting the velocity distributions, defined according to the probability density function [49],

$$\frac{1}{\pi\sigma}\exp\left[\frac{(1-\xi)^2}{2\sigma^2}\right]\int_{-\infty}^{\alpha(x-\xi)/\sigma} dt\exp\left(\frac{-t^2}{2}\right), \quad \text{(A1)}$$

with ξ the location parameter, σ the scale parameter, and α the shape parameter that determines the skewness. For barium (strontium), fitting yields distributions with a location parameter of 444 m/s (473 m/s), a scale parameter of 284 m/s (372 m/s), and a shape parameter of 2.0 (2.7).

During interference measurements, a lower wire current of 3.5–3.6 A was used to mitigate signal instabilities that appeared at higher temperatures. We also maximized the atomic flux by working with a large velocity spread, thus avoiding the use of narrow velocity-selecting delimiters. The combination of a moderate wire temperature and high flux allowed us to achieve the most stable interference patterns.

[1] J. H. V. Vleck, *The Theory of Electric and Magnetic Susceptibilities* (Oxford University Press, London, 1965).
[2] W. Gerlach and O. Stern, *Der Experimentelle Nachweis des Magnetischen Moments des Silberatoms*, Z. Phys. **8**, 110 (1922).
[3] I. I. Rabi, S. Millman, P. Kusch, and J. R. Zacharias, *The Molecular Beam Resonance Method for Measuring Nuclear Magnetic Moments. The Magnetic Moments of* $_3$Li^6, $_3$Li^7 *and* $_9$F^{19}, Phys. Rev. **55**, 526 (1939).
[4] H. Metcalf and P. v. d. Straten, *Laser Cooling and Trapping* (Springer, New York, 1999).

[5] D. Cox, D. Trevor, R. Whetten, E. Rohlfing, and A. Kaldor, *Aluminum Clusters: Magnetic Properties*, J. Chem. Phys. **84**, 4651 (1986).

[6] U. Rohrmann and R. Schafer, *Stern-Gerlach Experiments on* $Mn@Sn_{12}$*: Identification of a Paramagnetic Superatom and Vibrationally Induced Spin Orientation*, Phys. Rev. Lett. **111**, 133401 (2013).

[7] U. Rohrmann, P. Schwerdtfeger, and R. Schafer, *Atomic Domain Magnetic Nanoalloys: Interplay between Molecular Structure and Temperature Dependent Magnetic and Dielectric Properties in Manganese Doped Tin Clusters*, Phys. Chem. Chem. Phys. **16**, 23952 (2014).

[8] M. B. Knickelbein, *Magnetic Moments of Small Bimetallic Clusters:* Co_nMn_m, Phys. Rev. B **75**, 014401 (2007).

[9] M. B. Knickelbein, *Magnetic Ordering in Manganese Clusters*, Phys. Rev. B **70**, 014424 (2004).

[10] K. Miyajima, M. B. Knickelbein, and A. Nakajima, *Stern-Gerlach Study of Multidecker Lanthanide-Cyclooctatetraene Sandwich Clusters*, J. Phys. Chem. A **112**, 366 (2008).

[11] A. P. Wills and L. G. Hector, *The Magnetic Susceptibility of Oxygen, Hydrogen and Helium*, Phys. Rev. **23**, 209 (1924).

[12] G. G. Havens, *The Magnetic Susceptibilities of Some Common Gases*, Phys. Rev. **43**, 992 (1933).

[13] C. Barter, R. G. Meisenheimer, and D. P. Stevenson, *Diamagnetic Susceptibilities of Simple Hydrocarbons and Volatile Hydrides*, J. Phys. Chem. **64**, 1312 (1960).

[14] F. A. Jenkins and E. Segrè, *The Quadratic Zeeman Effect*, Phys. Rev. **55**, 52 (1939).

[15] R. J. Fonck, F. L. Roesler, D. H. Tracy, K. T. Lu, F. S. Tomkins, and W. R. S. Garton, *Atomic Diamagnetism and Diamagnetically Induced Configuration Mixing in Laser-Excited Barium*, Phys. Rev. Lett. **39**, 1513 (1977).

[16] D. R. Lide, *CRC Handbook of Chemistry and Physics*, 84th ed. (CRC Press, New York, 2004), pp. 4–130.

[17] M. M. Boyd, T. Zelevinsky, A. D. Ludlow, S. Blatt, T. Zanon-Willette, S. M. Foreman, and J. Ye, *Nuclear Spin Effects in Optical Lattice Clocks*, Phys. Rev. A **76**, 022510 (2007).

[18] L. Mairhofer, S. Eibenberger, A. Shayeghi, and M. Arndt, *A Quantum Ruler for Magnetic Deflectometry*, Entropy **20**, 516 (2018).

[19] Y. Y. Fein, P. Geyer, P. Zwick, F. Kiałka, S. Pedalino, M. Mayor, S. Gerlich, and M. Arndt, *Quantum Superposition of Molecules Beyond 25 kDa*, Nat. Phys. **15**, 1242 (2019).

[20] A. D. Cronin, J. Schmiedmayer, and D. E. Pritchard, *Optics and Interferometry with Atoms and Molecules*, Rev. Mod. Phys. **81**, 1051 (2009).

[21] W. Holmgren, M. Revelle, V. Lonij, and A. Cronin, *Absolute and Ratio Measurements of the Polarizability of Na, K, and Rb with an Atom Interferometer*, Phys. Rev. A **81**, 053607 (2010).

[22] L. Hackermüller, K. Hornberger, S. Gerlich, M. Gring, H. Ulbricht, and M. Arndt, *Optical Polarizabilities of Large Molecules Measured in Near-Field Interferometry*, Appl. Phys. B **89**, 469 (2007).

[23] S. Eibenberger, S. Gerlich, M. Arndt, J. Tüxen, and M. Mayor, *Electric Moments in Molecule Interferometry*, New J. Phys. **13**, 043033 (2011).

[24] S. Eibenberger, X. Cheng, J. P. Cotter, and M. Arndt, *Absolute Absorption Cross Sections from Photon Recoil in a Matter-Wave Interferometer*, Phys. Rev. Lett. **112**, 250402 (2014).

[25] L. Mairhofer, S. Eibenberger, J. P. Cotter, M. Romirer, A. Shayeghi, and M. Arndt, *Quantum-Assisted Metrology of Neutral Vitamins in the Gas Phase*, Angew. Chem. Int. Ed. **56**, 10947 (2017).

[26] T. Mazzoni, X. Zhang, R. Del Aguila, L. Salvi, N. Poli, and G. M. Tino, *Large-Momentum-Transfer Bragg Interferometer with Strontium Atoms*, Phys. Rev. A **92** (2015).

[27] L. Hu, N. Poli, L. Salvi, and G. M. Tino, *Atom Interferometry with the Sr Optical Clock Transition*, Phys. Rev. Lett. **119**, 263601 (2017).

[28] X. Zhang, R. P. del Aguila, T. Mazzoni, N. Poli, and G. M. Tino, *Trapped-Atom Interferometer with Ultracold Sr Atoms*, Phys. Rev. A **94**, 043608 (2016).

[29] R. P. del Aguila, T. Mazzoni, L. Hu, L. Salvi, G. M. Tino, and N. Poli, *Bragg Gravity-Gradiometer Using the* $^1S_0$–$^3P_1$ *Intercombination Transition of* ^{88}Sr, New J. Phys. **20**, 043002 (2018).

[30] J. Hartwig, S. Abend, C. Schubert, D. Schlippert, H. Ahlers, K. Posso-Trujillo, N. Gaaloul, W. Ertmer, and E. M. Rasel, *Testing the Universality of Free Fall with Rubidium and Ytterbium in a Very Large Baseline Atom Interferometer*, New J. Phys. **17**, 035011 (2015).

[31] M. G. Tarallo, T. Mazzoni, N. Poli, D. V. Sutyrin, X. Zhang, and G. M. Tino, *Test of Einstein Equivalence Principle for 0-Spin and Half-Integer-Spin Atoms: Search for Spin-Gravity Coupling Effects*, Phys. Rev. Lett. **113**, 023005 (2014).

[32] P. W. Graham, J. M. Hogan, M. A. Kasevich, and S. Rajendran, *New Method for Gravitational Wave Detection with Atomic Sensors*, Phys. Rev. Lett. **110**, 171102 (2013).

[33] A. O. Jamison, B. Plotkin-Swing, and S. Gupta, *Advances in Precision Contrast Interferometry with Yb Bose-Einstein Condensates*, Phys. Rev. A **90**, 063606 (2014).

[34] K. Patorski, in *Progress in Optics XXVII*, edited by E. Wolf (Elsevier Science Amsterdam, 1989), p. 1.

[35] K. Hornberger, S. Gerlich, P. Haslinger, S. Nimmrichter, and M. Arndt, *Colloquium: Quantum Interference of Clusters and Molecules*, Rev. Mod. Phys. **84**, 157 (2012).

[36] J. F. Clauser and S. Li, *Talbot-von Lau Atom Interferometry with Cold Slow Potassium*, Phys. Rev. A **49**, R2213 (1994).

[37] S. Eibenberger, S. Gerlich, M. Arndt, M. Mayor, and J. Tüxen, *Matter-Wave Interference of Particles Selected from a Molecular Library with Masses Exceeding 10 000 amu*, Phys. Chem. Chem. Phys. **15**, 14696 (2013).

[38] H. L. Schwartz, T. M. Miller, and B. Bederson, *Measurement of the Static Electric Dipole Polarizabilities of Barium and Strontium*, Phys. Rev. A **10**, 1924 (1974).

[39] M. K. Oberthaler, S. Bernet, E. M. Rasel, J. Schmiedmayer, and A. Zeilinger, *Inertial Sensing with Classical Atomic Beams*, Phys. Rev. A **54**, 3165 (1996).

[40] S. Nimmrichter and K. Hornberger, *Theory of Near-Field Interference Beyond the Eikonal Approximation*, Phys. Rev. A **78**, 023612 (2008).

[41] J. R. Cheeseman, G. W. Trucks, T. A. Keith, and M. J. Frisch, *A Comparison of Models for Calculating Nuclear*

Magnetic Resonance Shielding Tensors, J. Chem. Phys. **104**, 5497 (1996).

[42] M. J. Frisch *et al.*, Gaussian 16 Rev. C.01, 2016.

[43] C. Adamo and V. Barone, *Toward Reliable Density Functional Methods without Adjustable Parameters: The PBE0 Model*, J. Chem. Phys. **110**, 6158 (1999).

[44] F. Weigend and R. Ahlrichs, *Balanced Basis Sets of Split Valence, Triple Zeta Valence and Quadruple Zeta Valence Quality for H to Rn: Design and Assessment of Accuracy*, Phys. Chem. Chem. Phys. **7**, 3297 (2005).

[45] N. J. Stone, *Table of Nuclear Magnetic Dipole and Electric Quadrupole Moments*, At. Data Nucl. Data Tables **90**, 75 (2005).

[46] C. T. Sims, C. M. Craighead, R. I. Jaffe, D. N. Gideon, E. N. Wyler, F. C. Todd, D. M. Rosenbaum, E. M. Sherwood, and I. E. Campbell, *Investigations of Rhenium*, Report No. 54-371, 1954.

[47] M. D. Scheer and J. Fine, *Kinetics of Desorption. II.* Cs^+ *and* Ba^+ *from Rhenium*, J. Chem. Phys. **38**, 307 (1963).

[48] F. Stienkemeier, M. Wewer, F. Meier, and H. O. Lutz, *Langmuir–Taylor Surface Ionization of Alkali (Li, Na, K) and Alkaline Earth (Ca, Sr, Ba) Atoms Attached to Helium Droplets*, Rev. Sci. Instrum. **71**, 3480 (2000).

[49] A. Azzalini, *A Class of Distributions Which Includes the Normal Ones*, Scand. J. Stat. Theory Appl. **12**, 171 (1985).